

Production of light-flavor and single-charmed hadrons in pp collisions at $\sqrt{s} = 5.02$ TeV in an equal-velocity quark combination model

Hai-hong Li,¹ Feng-lan Shao,^{2,*} and Jun Song^{1,†}

¹*School of Physical Science and Intelligent Engineering, Jining University, Shandong 273155, China*

²*School of Physics and Physical Engineering, Qufu Normal University, Shandong 273165, China*

We apply an equal-velocity quark combination model to study the production of light-flavor hadrons and single-charmed hadrons at midrapidity in pp collisions at $\sqrt{s} = 5.02$ TeV. We find experimental data for p_T spectra of Ω and ϕ exhibit a quark number scaling property, which is a clear signal of quark combination mechanism at hadronization. Experimental data for p_T spectra of p , Λ , Ξ , Ω , ϕ and K^{*0} are systematically described by the model. The non-monotonic p_T dependence of Ω/ϕ ratio is naturally explained and we find it is closely related to the shape of the logarithm of strange quark p_T distribution. Using p_T spectra of light-flavor quarks obtained from light-flavor hadrons and a p_T spectrum of charm quarks which is consistent with perturbative QCD calculations, the experimental data for differential cross-sections of $D^{0,+}$, D_s^+ and Λ_c^+ as the function of p_T are systematically described. We predict the differential cross-sections of $\Xi_c^{0,+}$ and Ω_c^0 . The ratio $\Xi_c^{0,+}/D^0$ in our model is about 0.16 and Ω_c^0/D^0 is about 0.012 due to the cascade suppression of strangeness. In addition, the predicted $\Xi_c^{0,+}/D^0$ and Ω_c^0/D^0 ratios exhibit the non-monotonic dependence on p_T in the low p_T range.

I. INTRODUCTION

Recently, experiments of pp and pPb collisions at energies available at the CERN Large Hadron Collider (LHC) found a series of interesting properties of hadron production such as ridge and collectivity [1–4], enhancement of strangeness and ratios of baryon to meson [5–8]. These striking observations are possibly related to a hot topic in strong interactions, i.e., the formation of a small droplet of Quark-Gluon Plasma (QGP) in pp and pPb collisions. Theoretical studies along this direction are extensively carried out in the last few years from different aspects. The key point is how to understand and simulate the small final-state parton system created in pp and pPb collisions at LHC energies. These studies usually focus on the application of hydrodynamics to simulate mini-QGP evolution [9–16], the search of new features in string formation just before hadronization by various mechanisms such as color re-connection [17–21], the search of new features in string(cluster) fragmentation or parton(quark) coalescence mechanism at hadronization [22–27], etc.

In our recent studies on pp collisions at two collision energies $\sqrt{s} = 7, 13$ TeV [27–29] and on pPb collisions at $\sqrt{s_{NN}} = 5.02$ TeV [25, 30], we found that an equal-velocity combination mechanism of constituent quarks and antiquarks at hadronization can systematically describe the experimental data for p_T spectra of light-flavor hadrons and single-charmed hadrons in the low and intermediate p_T range in these collision systems. The constituent quark degrees of freedom just before hadronization play an important role for hadron production in these collisions, which may be related to possible formation of QGP droplet in pp and pPb collisions at LHC

energies. Compared with the traditional fragmentation mechanism usually applied in small collision systems, this quark-combination “new” feature at hadronization should be studied further with help of experimental data in pp and pPb collisions at other collision energies at LHC.

In this paper, we use an equal-velocity quark combination model to study the production of light-flavor hadrons and single-charmed hadrons in pp collisions at $\sqrt{s} = 5.02$ TeV. Firstly, we use the model to describe the experimental data of light-flavor hadrons [31–33]. We pay particular attention to how to systematically relate the observed properties of hadrons to quark p_T spectra at hadronization. For example, we correlate p_T spectrum of Ω and that of ϕ by a scaling method to directly relate to p_T distribution of strange quarks at hadronization. Another example is that we can relate the non-monotonic p_T dependence of Ω/ϕ ratio to the shape of the logarithm of strange quark distribution. Second, using p_T spectra of light-flavor quarks obtained from study of light-flavor hadrons and a charm quark distribution which is consistent with perturbative QCD calculations, we further study the equal-velocity combination of light-flavor and charm (anti-)quarks to explain the production properties of single-charmed hadrons. We compare model results with experimental data for differential cross-sections of $D^{0,+}$, D_s^+ and Λ_c^+ [34, 35]. We predict the differential cross-sections of $\Xi_c^{0,+}$ and Ω_c^0 and several baryon to meson ratios such as $\Xi_c^{0,+}/D^0$ and Ω_c^0/D^0 for the future test.

The paper is organized as follows. In Sec. II, we briefly introduce a particular quark combination model under equal-velocity combination approximation. In Sec. III, we show results for p_T spectra of light-flavor hadrons in pp collisions at $\sqrt{s} = 5.02$ TeV. In Sec. IV, we show results for p_T spectra and spectrum ratios of single-charmed hadrons. In Sec. V, we give the summary.

* shaofl@mail.sdu.edu.cn

† songjun2011@jnxu.edu.cn

II. A BRIEF INTRODUCTION OF EQUAL-VELOCITY QUARK COMBINATION MODEL

In this section, we briefly introduce a particular quark combination model proposed in recent work [25]. This model applies a simplified combination criterion, i.e., the equal-velocity combination (EVC), to determine how constituent quarks and antiquarks at hadronization form hadrons. This EVC model was inspired by the quark number scaling property found in p_T spectra of strange hadrons [25, 29]. The model has successfully described p_T spectra of light-flavor hadrons and single-charmed hadrons in ground state in pp collisions at $\sqrt{s} = 7, 13$ TeV and in pPb collisions at $\sqrt{s_{NN}} = 5.02$ TeV. Our latest studies on elliptic flow and p_T spectra of hadrons in relativistic heavy-ion collisions [36–39] also support the EVC model.

In the scenario of stochastic combination of quarks and antiquarks at hadronization, momentum distribution of the formed hadron $f_h(p) \equiv dN_h/dp$ can be constructed by those of quarks and antiquarks,

$$f_{B_j}(p_B) = \int dp_1 dp_2 dp_3 \mathcal{R}_{B_j}(p_1, p_2, p_3; p_B) f_{q_1 q_2 q_3}(p_1, p_2, p_3) \text{with} \quad (1)$$

$$f_{M_j}(p_M) = \int dp_1 dp_2 \mathcal{R}_{M_j}(p_1, p_2; p_M) f_{q_1 \bar{q}_2}(p_1, p_2), \quad (2)$$

where $f_{q_1 q_2 q_3}(p_1, p_2, p_3)$ and $f_{q_1 \bar{q}_2}(p_1, p_2)$ are joint momentum distributions for $q_1 q_2 q_3$ and $q_1 \bar{q}_2$, respectively. $\mathcal{R}_{B_j}(p_1, p_2, p_3; p_B)$ is the combination probability function for three quarks $q_1 q_2 q_3$ with momenta p_1, p_2 and p_3 forming a baryon B_j with quark composition $q_1 q_2 q_3$ and momentum p_B . $\mathcal{R}_{M_j}(p_1, p_2; p_M)$ has similar meaning.

Under the approximation of EVC, a hadron is formed by the combination of constituent quarks and/or antiquarks with same velocity. Because momentum has property $p_i = \gamma m_i v \propto m_i$ at the given velocity, the momentum of the participant (anti-)quark p_i should have a particular fraction $x_i = p_i/p \propto m_i$ of the momentum of hadron p where m_i is the constituent mass of the quark i . Considering the momentum conservation $\sum_i p_i = p$ we obtain

$$x_i = \begin{cases} \frac{m_i}{m_1+m_2+m_3} & i = 1, 2, 3 \text{ for } B(q_1 q_2 q_3) \\ \frac{m_i}{m_1+m_2} & i = 1, 2 \text{ for } M(q_1 \bar{q}_2) \end{cases}. \quad (3)$$

The constituent masses of quarks are taken as $m_u = m_d = 0.3$ GeV, $m_s = 0.5$ GeV and $m_c = 1.5$ GeV. The combination function therefore has the simple form

$$\mathcal{R}_{B_j}(p_1, p_2, p_3; p_B) = \kappa_{B_j} \prod_{i=1}^3 \delta(p_i - x_i p_B), \quad (4)$$

$$\mathcal{R}_{M_j}(p_1, p_2; p_M) = \kappa_{M_j} \prod_{i=1}^2 \delta(p_i - x_i p_M). \quad (5)$$

κ_{B_j} and κ_{M_j} are independent of momentum but can be dependent on numbers of (anti-) quarks at hadronization and the property of the formed hadron such as spin.

Substituting combination functions Eqs. (4) and (5) into Eqs. (1) and (2), we obtain

$$f_{B_j}(p_B) = \kappa_{B_j} f_{q_1 q_2 q_3}(x_1 p_B, x_2 p_B, x_3 p_B), \quad (6)$$

$$f_{M_j}(p_M) = \kappa_{M_j} f_{q_1 \bar{q}_2}(x_1 p_M, x_2 p_M). \quad (7)$$

Integrating above equations over the momentum, we obtain the number of the formed hadrons

$$N_{B_j} = \kappa_{B_j} \int dp_B f_{q_1 q_2 q_3}(x_1 p_B, x_2 p_B, x_3 p_B), \quad (8)$$

$$N_{M_j} = \kappa_{M_j} \int dp_M f_{q_1 \bar{q}_2}(x_1 p_M, x_2 p_M). \quad (9)$$

The integral of joint momentum distribution of (anti-)quarks can be rewritten as

$$\int dp_B f_{q_1 q_2 q_3}(x_1 p_B, x_2 p_B, x_3 p_B) = \frac{N_{q_1 q_2 q_3}}{A_{B_j}}, \quad (10)$$

$$\int dp_M f_{q_1 \bar{q}_2}(x_1 p_M, x_2 p_M) = \frac{N_{q_1 \bar{q}_2}}{A_{M_j}} \quad (11)$$

$$N_{q_1 q_2 q_3} = \iiint dp_1 dp_2 dp_3 f_{q_1 q_2 q_3}(p_1, p_2, p_3), \quad (12)$$

$$N_{q_1 \bar{q}_2} = \iint dp_1 dp_2 f_{q_1 \bar{q}_2}(p_1, p_2). \quad (13)$$

Here, $N_{q_1 \bar{q}_2}$ is the number of all $q_1 \bar{q}_2$ pairs at hadronization. In general, we have $N_{q_1 \bar{q}_2} = N_{q_1} N_{\bar{q}_2}$ where N_{q_1} is the number of q_1 in system and $N_{\bar{q}_2}$ is that of \bar{q}_2 . $N_{q_1 q_2 q_3}$ is the number of all possible $q_1 q_2 q_3$ combinations. In general, $N_{q_1 q_2 q_3}$ equals to $N_{q_1} N_{q_2} N_{q_3}$ for different quark flavors, $N_{q_1}(N_{q_1} - 1)N_{q_2}$ for two identical quark flavor and $N_{q_1}(N_{q_1} - 1)(N_{q_1} - 2)$ for three identical quark flavor. Coefficients A_{B_j} and A_{M_j} are thus introduced to characterize the effect of joint momentum distribution of (anti-)quarks with correlated momenta on the number of the formed hadron.

Substituting Eqs. (10) and (11) into Eqs. (8) and (9), we obtain

$$N_{B_j} = N_{q_1 q_2 q_3} \frac{\kappa_{B_j}}{A_{B_j}} = N_{q_1 q_2 q_3} P_{q_1 q_2 q_3 \rightarrow B_j}, \quad (14)$$

$$N_{M_j} = N_{q_1 \bar{q}_2} \frac{\kappa_{M_j}}{A_{M_j}} = N_{q_1 \bar{q}_2} P_{q_1 \bar{q}_2 \rightarrow M_j}. \quad (15)$$

Coefficient ratio κ_{B_j}/A_{B_j} thus has an intuitive physical meaning, that is, the momentum-integrated probability of $q_1 q_2 q_3$ forming a B_j . Therefore, we denote it as $P_{q_1 q_2 q_3 \rightarrow B_j}$ in the second equality. κ_{M_j}/A_{M_j} denotes the momentum-integrated probability of a $q_1 \bar{q}_2$ pair forming a M_j , and we denote it as $P_{q_1 \bar{q}_2 \rightarrow M_j}$.

Because of the non-perturbative nature of $P_{q_1 q_2 q_3 \rightarrow B_i}$ and $P_{q_1 \bar{q}_2 \rightarrow M_i}$, we will parameterize them in the following

text. Here, we consider the formation of hadrons in two sectors. One is light-flavor hadrons which are exclusively composed of light-flavor (anti-)quarks. Another is single-charmed hadrons which are composed of a charm (anti-)quark and light-flavor (anti-)quark(s). For convenience, light-flavor quarks are denoted as l_i ($l_i = d, u, s$) and N_{l_i} their numbers. The number of all light-flavor quarks is $N_l = \sum_{l_i} N_{l_i}$ and similar for anti-quarks. Charm quarks are denoted as c and N_c its number.

Considering the stochastic feature of the quark combination and flavor independence of strong interaction, the combination probability of light-flavor (anti-)quarks can be parameterized by

$$P_{l_1 l_2 l_3 \rightarrow B_j} = C_{B_j} N_{iter} \frac{\overline{N}_B}{N_{lll}}, \quad (16)$$

$$P_{l_1 \bar{l}_2 \rightarrow M_j} = C_{M_j} \frac{\overline{N}_M}{N_{l\bar{l}}}, \quad (17)$$

where we use \overline{N}_B/N_{lll} to denote the average probability of three light-flavor quarks combining into a baryon and $\overline{N}_M/N_{l\bar{l}}$ to denote the average probability of a light-flavor quark and antiquark pair combining into a meson. Here, \overline{N}_B and \overline{N}_M are the average number of all light-flavor baryons and that of all mesons. $N_{lll} = N_l(N_l - 1)(N_l - 2)$ is the number of all possible three quark combinations and $N_{l\bar{l}} = N_l N_{\bar{l}}$ is the number of all possible light-flavor quark antiquark pairs. N_{iter} is number of permutation for $l_1 l_2 l_3$ and is taken as 6 for three different flavors and 3 for two identical flavor and 1 for three identical flavor, respectively.

C_{B_j} and C_{M_j} are introduced to tune the production weight of hadrons with same quark content but different spins. In this paper, we only consider the ground state $J^P = 0^-, 1^-$ mesons and $J^P = (1/2)^+, (3/2)^+$ baryons in flavor SU(3) group. We introduce a parameter $R_{V/P}$ to denote the relative production weight of the vector mesons to the pseudoscalar mesons with the same flavor composition. Then, we get $C_{M_j} = 1/(1 + R_{V/P})$ for $J^P = 0^-$ mesons and $C_{M_j} = R_{V/P}/(1 + R_{V/P})$ for $J^P = 1^-$ mesons. Similarly, we introduce a parameter $R_{D/O}$ to denote the relative production weight of the decuplet baryons to the octet baryons with the same flavor composition. Then, we have $C_{B_j} = 1/(1 + R_{D/O})$ for $J^P = (1/2)^+$ baryons and $C_{B_j} = R_{D/O}/(1 + R_{D/O})$ for $J^P = (3/2)^+$ baryons, except $C_\Lambda = C_{\Sigma^0} = 1/(2 + R_{D/O})$, $C_{\Sigma^{*0}} = R_{D/O}/(2 + R_{D/O})$, $C_{\Delta^{++}} = C_{\Delta^-} = C_{\Omega^-} = 1$. Here, $R_{V/P}$ and $R_{O/D}$ are set to be 0.45 and 0.5, respectively, according to our recent work in pp collisions at $\sqrt{s} = 13$ TeV [29].

Similar to Eqs. (16) and (17), the combination probability of a charm quark and light-flavor (anti-)quark(s) can be parameterized by

$$P_{cl_1 l_2 \rightarrow B_j} = C_{B_j} N_{iter} \frac{\overline{N}_{Bc}}{N_{c ll}}, \quad (18)$$

$$P_{c \bar{l}_1 \rightarrow M_j} = C_{M_j} \frac{\overline{N}_{M_c}}{N_{c \bar{l}}}, \quad (19)$$

where $N_{c ll} = N_c N_l (N_l - 1)$, $N_{c \bar{l}} = N_c N_{\bar{l}}$ and N_{iter} equals to 1 as $l_1 = l_2$ or 2 as $l_1 \neq l_2$. In this paper, we consider the ground state $J^P = 0^-, 1^-$ single-charmed mesons, $J^P = (1/2)^+$ triplet and sextet single-charmed baryons, and $J^P = (3/2)^+$ sextet single-charmed baryons. Similar to light-flavor mesons, we introduce the parameter $R'_{V/P}$ to denote the relative production weight of the vector mesons to the pseudoscalar mesons. Different from light-flavor baryons, we introduce two parameters in single-charmed baryons. We use a parameter $R_{S1/T}$ to denote the relative production weight of $J^P = (1/2)^+$ sextet baryons to $J^P = (1/2)^+$ triplet baryons with the same flavor composition, and another parameter $R_{S3/S1}$ to denote that of $J^P = (3/2)^+$ sextet baryons to $J^P = (1/2)^+$ sextet baryons. We take $R'_{V/P} = 1.5$, $R_{S1/T} = 0.5$ and $R_{S3/S1} = 1.4$ according to our previous work of single-charmed hadrons [30]. We emphasize that yields and momentum spectra of final state charmed baryons Λ_c^+ , $\Xi_c^{0,+}$ and Ω_c^0 after taking strong and electromagnetic decays into account are actually insensitive to parameters $R_{S1/T}$ and $R_{S3/S1}$.

The unitarity of the hadronization process constrains the number of the formed hadrons,

$$\overline{N}_M + 3\overline{N}_B + \overline{N}_{M_c} + 2\overline{N}_{B_c} = N_l, \quad (20)$$

$$\overline{N}_M + 3\overline{N}_B + \overline{N}_{M_c} + 2\overline{N}_{B_c} = N_{\bar{l}}, \quad (21)$$

$$\overline{N}_{M_c} + \overline{N}_{B_c} = N_c, \quad (22)$$

$$\overline{N}_{M_c} + \overline{N}_{B_c} = N_{\bar{c}}, \quad (23)$$

where we neglect the contribution of multi-charmed hadrons. Because of small value for the relative production ratio $N_c/N_l \sim \mathcal{O}(1\%)$ in high energy pp , pA and AA collisions, we can neglect the contribution of charmed hadrons in Eqs. (20) and (21) and then obtain the separate constraint for N_l and N_c , respectively.

In collisions at LHC energies, the approximation of charge conjugation symmetry $N_{q_i} = N_{\bar{q}_i}$ and $N_h = N_{\bar{h}}$ is usually satisfied. Therefore, the above unitarity constraints are reduced to $\overline{N}_M + 3\overline{N}_B \approx N_l$ and $\overline{N}_{M_c} + \overline{N}_{B_c} = N_c$. We can define the competition factor $R_{B/M} = \overline{N}_B/\overline{N}_M$ to quantify the production weight of baryons in light-flavor sector and take it as a model parameter. Then we can calculate

$$\overline{N}_B = \frac{R_{B/M}}{1 + 3R_{B/M}} N_l, \quad (24)$$

$$\overline{N}_M = \frac{1}{1 + 3R_{B/M}} N_l. \quad (25)$$

We found that $R_{B/M} = 0.087 \pm 0.04$ can well explain data of yield densities of light-flavor hadrons in relativistic heavy-ion collisions at RHIC and LHC energies and those in pp and pPb collisions at LHC energies [38, 40, 41]. We also define a competition factor $R_{B/M}^{(c)}$ for single-charmed

hadrons and obtain

$$\bar{N}_{B_c} = \frac{R_{B/M}^{(c)}}{1 + R_{B/M}^{(c)}} N_c, \quad (26)$$

$$\bar{N}_{M_c} = \frac{1}{1 + R_{B/M}^{(c)}} N_c. \quad (27)$$

We found that $R_{B/M}^{(c)}$ is about 0.425 ± 0.025 in our recent works [27, 30] by fitting the midrapidity data of Λ_c^+ in pp collisions at $\sqrt{s} = 7$ TeV and those in pPb collisions at $\sqrt{s_{NN}} = 5.02$ TeV measured by ALICE collaboration [42].

Quark momentum distributions $f_{q_1 q_2 q_3}(p_1, p_2, p_3)$ and $f_{q_1 \bar{q}_2}(p_1, p_2)$ are inputs of the model. When they are given, we can obtain $N_{q_1 q_2 q_3}$, $N_{q_1 \bar{q}_2}$, N_{q_i} and $N_{\bar{q}_i}$ after integrating over momenta. Then, substituting Eqs. (24-25) into Eqs. (16-17) and subsequently substituting the latter into Eqs. (14-15), we can obtain yields of light-flavor hadrons. By Eqs. (14-15) and Eqs. (10-11), we can calculate coefficients κ_{B_j} and κ_{M_j} . Substituting them into Eqs. (6-7), we can obtain momentum distributions of light-flavor hadrons. Calculations of single-charmed hadron are similar.

We also consider the physical situation that the numbers of quarks are not fixed values but are fluctuated event by event in high energy collisions. As we did in Ref. [41], we consider the Poisson distribution as the base line to simulate the numbers of quarks of different kinds of flavors produced in midrapidity range in each event. Then we take the event average of the numbers of hadrons to obtain their yield densities. We note that the effect of quark number fluctuations influences little on production of mesons and weakly on that of baryons containing up and down quarks but obviously on that of multi-strange baryons such as Ω [41]. The fluctuations for momentum distributions of quarks are not considered at the moment.

We finally consider the decay effects of short-life hadrons on production of stable hadrons,

$$f_{h_j}^{(final)}(p) = f_{h_j}(p) + \sum_{i \neq j} \int dp' f_{h_i}(p') D_{ij}(p', p), \quad (28)$$

where the decay function $D_{ij}(p', p)$ is calculated by decay kinetics and decay branch ratios reported by Particle Data Group [43].

As a short summary of this section, we emphasize that the EVC model is essentially a statistical model based on the constituent quark degrees of freedom at hadronization. In deriving momentum spectra and yields of hadrons, stochastic feature of quark combination and flavor-independence of strong interactions are mainly used. The effect of flavor symmetry broken is taken into account, on the one hand, by the difference in momentum distributions (and also numbers) of quarks with different flavors which will be discussed in the following text, and on the other hand, by the flavor-dependent parameter

such as the difference between $R_{B/M}$ in light-flavors and $R_{B/M}^{(c)}$ in charms. In addition, non-perturbative dynamics in combination process which are difficult to be calculated in first principles are parameterized in the model. We expect that values of these parameters such as $R_{V/P}$ and $R_{B/M}$ are stable in different high energy collisions, as indicated by our available studies up to now. Finally, the momentum distribution $dN_{h,q}/dp$ is a general denotation. In this paper, we focus on the transverse production of hadrons at midrapidity, then the momentum distribution $dN_{h,q}/dp$ refers to $dN_{h,q}/dp_T dy$ at midrapidity.

III. RESULTS OF LIGHT-FLAVOR HADRONS

In our model, momentum distributions of light-flavor constituent quarks at hadronization are inputs. Because they are difficult to be calculated in the low p_T range from first principles, we determine them by fitting experimental data of identified hadrons in our model. Considering that the available experimental measurements are mainly inclusive distribution, here we assume the factorization approximation for the joint momentum distribution of (anti-)quarks, i.e., $f_{q_1 q_2 q_3}(p_{T_1}, p_{T_2}, p_{T_3}) = f_{q_1}(p_{T_1}) f_{q_2}(p_{T_2}) f_{q_3}(p_{T_3})$ and $f_{q_1 \bar{q}_2}(p_{T_1}, p_{T_2}) = f_{q_1}(p_{T_1}) f_{\bar{q}_2}(p_{T_2})$. In addition, we take the isospin symmetry $f_u(p_T) = f_d(p_T)$ and the charge-conjugation symmetry $f_{q_i}(p_T) = f_{\bar{q}_i}(p_T)$ for p_T spectra of (anti-)quarks at midrapidity at LHC energies. Finally, we have only two inputs $f_u(p_T)$ and $f_s(p_T)$ in light-flavor sector which can be conveniently determined by experimental data of a few of hadrons.

In this section, we study the production of light-flavor hadrons in the low and intermediate p_T range at midrapidity in pp collisions at $\sqrt{s} = 5.02$ TeV. In particular, we discuss a quark number scaling property for p_T spectra of Ω^- and ϕ and study the p_T dependence of Ω/ϕ ratio. We also study the property of the extracted p_T spectra of up quarks and strange quarks.

A. Scaling property for p_T spectra of Ω^- and ϕ

In this subsection, we discuss an interesting correlation between p_T spectrum of Ω^- and that of ϕ , which gives a first insight into hadron production mechanism at hadronization. Ω and ϕ consist of strange quarks/antiquarks, exclusively. In EVC model, p_T spectra of Ω^- and ϕ have simple expressions

$$f_{\Omega}(3p_T) = \kappa_{\Omega} [f_s(p_T)]^3, \quad (29)$$

$$f_{\phi}(2p_T) = \kappa_{\phi} f_s(p_T) f_{\bar{s}}(p_T) = \kappa_{\phi} [f_s(p_T)]^2, \quad (30)$$

where we use $f_s(p_T) = f_{\bar{s}}(p_T)$ for midrapidity at LHC energy. We then obtain the following correlation

$$f_{\phi}^{1/2}(2p_T) = \kappa_{\phi, \Omega} f_{\Omega}^{1/3}(3p_T) \quad (31)$$

where the coefficient $\kappa_{\phi,\Omega} = \kappa_{\phi}^{1/2}/\kappa_{\Omega}^{1/3}$ is independent of p_T . Eq. (31) means that, in the stochastic combination scenario of quarks and antiquarks at hadronization, p_T spectra of Ω^- and ϕ have a strong correlation based on the number of strange (anti-)quarks they contain. Therefore, we call Eq. (31) the quark number scaling property.

In Fig. 1, we test Eq. (31) by the preliminary data of p_T spectrum of ϕ in the rapidity interval $|y| < 0.5$ in inelastic events in pp collisions at $\sqrt{s} = 5.02$ TeV measured by ALICE collaboration [31] and data of Ω (i.e., $\Omega^- + \bar{\Omega}^+$) in the rapidity interval $|y| < 1.8$ in minimum-bias events measured by CMS collaboration [33]. In order to compare the scaled data from two different collaborations, the coefficient $\kappa_{\phi,\Omega}$ is taken as 1.58 but not the direct calculation of our model¹. We see that the scaled data of Ω are in good agreement with those of ϕ . Furthermore, we know from Eqs. (29) and (30) that Eq. (31) equals to $f_s(p_T)$ multiplying by a p_T -independent coefficient $\sqrt{\kappa_{\phi,\Omega}}$. Therefore, Fig. 1 also gives the direct information on the p_T spectrum of strange quarks at hadronization in pp collisions at $\sqrt{s} = 5.02$ TeV.

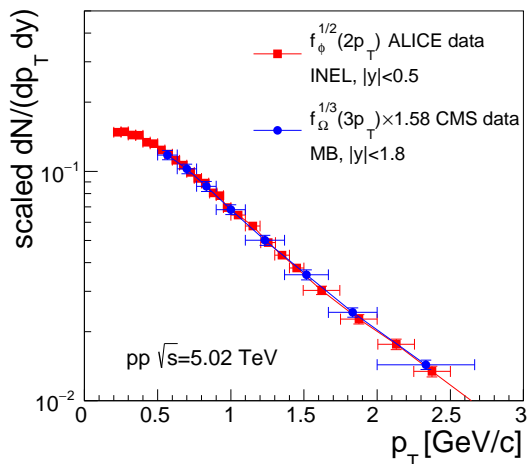


Figure 1. The scaled p_T spectra of Ω and ϕ in pp collisions at $\sqrt{s} = 5.02$ TeV. Experimental data of Ω and ϕ are from [31, 33].

B. p_T spectra of p , K^{*0} , Λ and Ξ

We parameterize the p_T spectrum of quarks by a Lévy-Tsallis functional form [44]. According to Eq. (30), we can use our model to fit the scaled data of ϕ in Fig. 1 to obtain the p_T spectrum of strange quarks $f_s(p_T)$ at hadronization. We further use the model to fit experimental data of p_T spectrum of proton [32] to obtain the p_T spectrum of up/down quarks $f_u(p_T)$ at hadronization. The properties of $f_s(p_T)$ and $f_u(p_T)$ will be discussed in Sec. III D.

When $f_u(p_T)$ and $f_s(p_T)$ are obtained, we can calculate p_T spectra of various light-flavor hadrons. In Fig. 2(b), we show the result for p_T spectrum of

$(K^{*0} + \bar{K}^{*0})/2$ and compare it with the experimental data [45]. We see a good agreement. Note that data of ϕ , proton and K^* are all ALICE data in inelastic events and rapidity interval $|y| < 0.5$. In Fig. 2 (c) and (d), we present results of $\Lambda + \bar{\Lambda}$ and $\Xi^- + \bar{\Xi}^+$ and compare them with experimental data of CMS collaboration [33]. Because CMS experiments select the minimum-bias events and rapidity interval $|y| < 1.8$ which are different from ALICE experiments, we multiply our results of Λ and Ξ by a constant 0.85 to test the shape of p_T distributions of hyperons predicted in our model¹. We see a good description for the shape of p_T spectra of two hyperons.

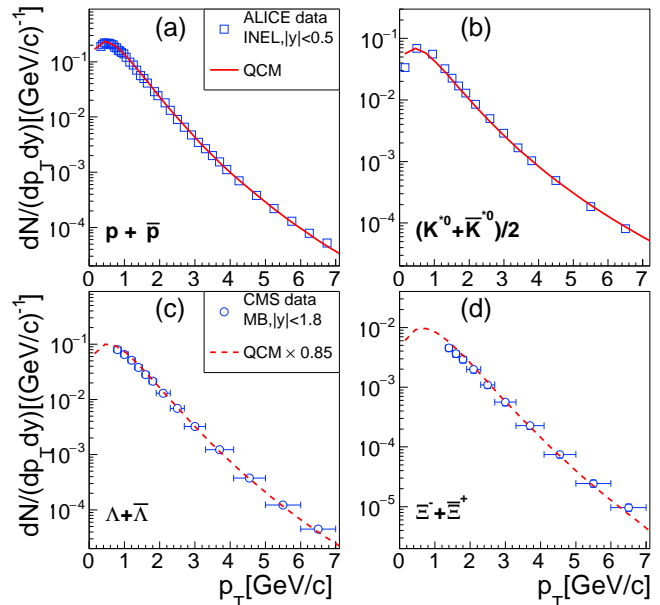


Figure 2. p_T spectra of $p + \bar{p}$, $(K^{*0} + \bar{K}^{*0})/2$, $\Lambda + \bar{\Lambda}$ and $\Xi^- + \bar{\Xi}^+$ in pp collisions at $\sqrt{s} = 5.02$ TeV. Symbols are experimental data [32, 33, 45] and lines with label “QCM” are model results.

C. Ratio Ω/ϕ as the function of p_T

In Fig. 3(a), we show the fitting result for p_T spectrum of ϕ and the calculation result for p_T spectrum of Ω (i.e., $\Omega^- + \bar{\Omega}^+$) in pp collisions at $\sqrt{s} = 5.02$ TeV. Similar to the case of Λ and Ξ in Fig. 2, we also multiply our result of Ω by a constant 0.85 in order to compare with

¹ By examining the available experimental data for p_T spectra of hyperons in pp collisions at $\sqrt{s} = 7$ TeV measured by ALICE collaboration and those by CMS collaboration [46–48], we notice that the average transverse momentum $\langle p_T \rangle$ and the shape of p_T distributions measured by two collaborations are quite consistent, although the center values of dN/dy measured by two collaborations have a certain difference. Therefore, in this paper, we put two data sets in pp collisions at $\sqrt{s} = 5.02$ TeV into together to test our model.

the shape of experimental data for p_T spectrum of Ω measured by CMS collaboration [33]. As indicated by the quark number scaling property in Fig. 1, we see that p_T spectra of ϕ and Ω can be simultaneously described by our model.

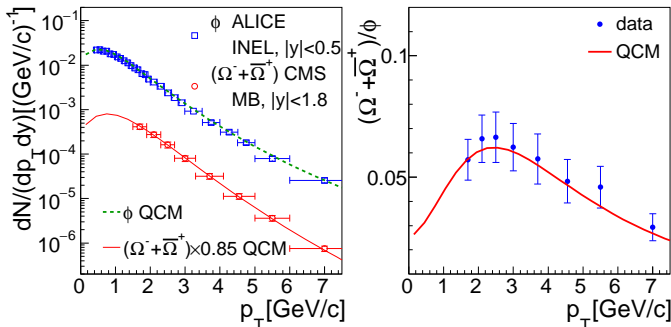


Figure 3. (a) p_T spectra of Ω and ϕ in pp collisions at $\sqrt{s} = 5.02$ TeV. (b) ratio Ω/ϕ as the function of p_T . Lines with label “QCM” are model results and symbols are experimental data [31, 33].

In Fig. 3(b), we show the result for Ω/ϕ ratio as the function of p_T and compare with experimental data. Here, the experimental data for Ω/ϕ ratio are calculated by data of their inclusive p_T spectra in Fig. 3 (a) with the propagation of statistical uncertainties [31, 33]. We see that ratio Ω/ϕ firstly increases with p_T in the low p_T range ($p_T \lesssim 2.5$ GeV/c) and then turns to decrease with p_T at larger p_T . Our model result, the solid line, well explains experimental data.

This non-monotonic p_T dependence of the ratio of baryon to meson and, in particular, the enhancement in the low p_T range have been observed many times in relativistic heavy-ion collisions [49–53] and in pp and pPb collisions at LHC energies [8, 46, 54]. This typical behavior of baryon to meson ratio is usually regarded as the consequence of the quark combination mechanism at hadronization [55–59]. In this paper, taking Ω/ϕ ratio as an example, we carry out a simple derivation to further clarify the underlying physics of such p_T dependence of baryon to meson ratios in the low and intermediate p_T range.

To understand the p_T dependence of Ω/ϕ ratio, we calculate the slope of the ratio

$$\begin{aligned} & \left[\frac{f_\Omega(p_T)}{f_\phi(p_T)} \right]' \\ &= \frac{f_\Omega(p_T)}{f_\phi(p_T)} \left[\frac{f'_\Omega(p_T)}{f_\Omega(p_T)} - \frac{f'_\phi(p_T)}{f_\phi(p_T)} \right] \\ &= \frac{f_\Omega(p_T)}{f_\phi(p_T)} \left[\frac{\partial \ln(f_s(p_T/3))}{\partial(p_T/3)} - \frac{\partial \ln(f_s(p_T/2))}{\partial(p_T/2)} \right]. \end{aligned} \quad (32)$$

Using the mean-value theorem, the term in bracket in the

last line becomes

$$\begin{aligned} & \frac{\partial \ln(f_s(p_T/3))}{\partial(p_T/3)} - \frac{\partial \ln(f_s(p_T/2))}{\partial(p_T/2)} \\ &= -\frac{1}{6} p_T [\ln f_s(\xi)]'' \end{aligned} \quad (33)$$

with $p_T/3 < \xi < p_T/2$. Finally, we have

$$\left[\ln \frac{f_\Omega(p_T)}{f_\phi(p_T)} \right]' = -\frac{1}{6} p_T [\ln f_s(\xi)]'', \quad (34)$$

which means that the slope of the Ω/ϕ ratio is influenced by the second derivative of the logarithm of strange quark distribution.

The second derivative of a distribution is related to that this distribution is convex or concave in shape. This can be conveniently read from Fig. 1 or Fig. 4. We see that $[\ln f_s(p_{T,s})]'' < 0$ as $p_{T,s} \lesssim 0.9$ GeV/c and $[\ln f_s(p_{T,s})]'' > 0$ as $1.0 \lesssim p_{T,s} \lesssim 2.5$ GeV/c. Therefore, the Ω/ϕ ratio increases with p_T in the range $p_T \lesssim 2 - 3$ GeV/c and decreases with p_T at larger p_T .

As we know, quarks of small p_T mainly come from soft QCD process and p_T distribution of these quarks is usually described by a thermal-like function $\exp[-\sqrt{p_T^2 + m^2}/T]$ which just has the property $[\ln f_s(p_{T,s})]'' < 0$ leading to the increase of Ω/ϕ ratio. Quarks of large p_T mainly come from hard QCD process and p_T distribution of these quarks is usually described by a jet-like function $(1 + p_T/p_0)^{-n}$ with $p_0 > 0$ and $n > 0$ which just has the property $[\ln f_s(p_{T,s})]'' > 0$ leading to the decrease of Ω/ϕ ratio. Therefore, we emphasize that the observed non-monotonic p_T dependence of the Ω/ϕ ratio not only depends on quark combination mechanism but also depends on the property of the momentum distribution of strange quarks at hadronization.

D. Difference between u and s quarks in p_T spectrum

In Fig. 4(a), we show the p_T spectra of up and strange quarks at hadronization extracted from data of ϕ and proton in inelastic pp collisions at $\sqrt{s} = 5.02$ TeV. The ratio in p_T -integrated yield density between strange quarks and up quarks, i.e., strangeness suppression factor,

$$\lambda_s = \frac{dN_s/dy}{dN_u/dy} \quad (35)$$

is about 0.3. In panel (b), we show the spectrum ratio of strange quarks to up quarks. We see that the ratio increases with p_T as $p_T \lesssim 1$ GeV/c and turns to weakly decrease at larger p_T . We note that this property is also observed in pp collisions at other collision energies and in relativistic heavy-ion collisions [25, 29, 38].

The difference in the p_T spectrum between up quarks and strange quarks will influence p_T spectra of the formed

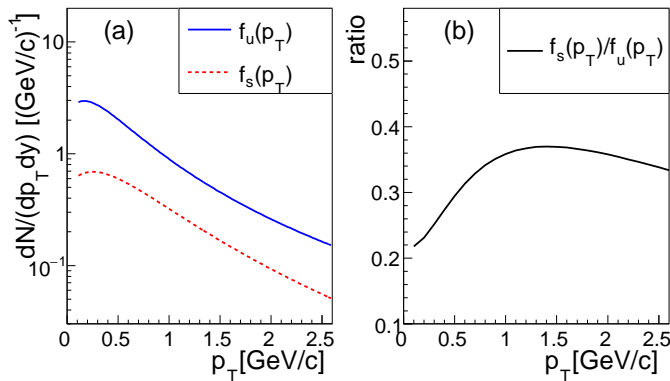


Figure 4. (a) p_T spectra of up and strange quarks at hadronization in inelastic pp collisions at $\sqrt{s} = 5.02$ TeV. (b) the ratio $f_s(p_T)/f_u(p_T)$.

hadrons with different strange quark content. In Fig. 5, we show ratios $(\Lambda + \bar{\Lambda})/(p + \bar{p})$, $(\Xi^- + \bar{\Xi}^+)/(\Lambda + \bar{\Lambda})$, and $(\Omega^- + \bar{\Omega}^+)/(\Xi^- + \bar{\Xi}^+)$ as the function of p_T . Symbols are experimental data and different kinds of lines are model results. The experimental data of three ratios are calculated by data of their inclusive p_T spectra with propagation of statistical uncertainties [32, 33]. We see that data of three ratios in the low p_T range ($p_T \lesssim 4$ GeV/c) all increase with p_T . In our model, this is because of the quark level property shown in Fig. 4(b) as $p_{T,q} \lesssim 1.3$ GeV/c. The hierarchy in magnitude for data of three ratios can be understood in our model by ratios of yield densities,

$$\frac{dN_\Lambda/dy}{dN_p/dy} \approx \frac{7.7}{4} \lambda_s, \quad (36)$$

$$\frac{dN_\Xi/dy}{dN_\Lambda/dy} \approx \frac{3}{7.7} \lambda_s, \quad (37)$$

$$\frac{dN_\Omega/dy}{dN_\Xi/dy} \approx \frac{1}{3} \lambda_s, \quad (38)$$

where coefficients before λ_s are due to the iteration factor N_{iter} in Eq. (16) and strong/electromagnetic decay contribution of decuplet baryons, see [29, 60] for the detailed analytical expressions of their yields.

IV. RESULTS OF CHARMED HADRONS

In this section, we study the production of single-charmed hadrons in pp collisions at $\sqrt{s} = 5.02$ TeV. We firstly extract the p_T spectrum of charm quarks and compare it with the calculation result of perturbative QCD method. Then, we present results of D mesons and Λ_c^+ baryon, and we compare them with experimental data. We also predict the p_T -differential cross-section of $\Xi_c^{0,+}$ and Ω_c^0 , and their ratios to D mesons as the function of p_T .

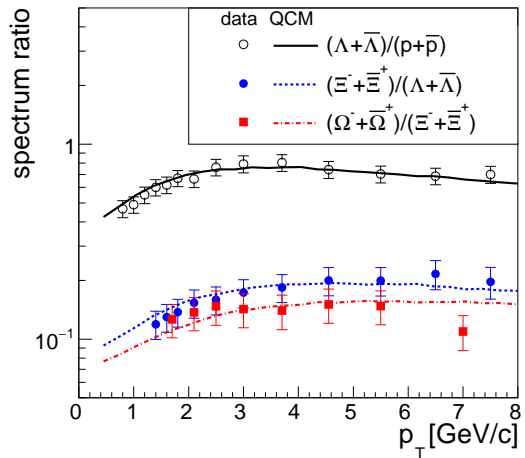


Figure 5. Spectrum ratios $(\Lambda + \bar{\Lambda})/(p + \bar{p})$, $(\Xi^- + \bar{\Xi}^+)/(\Lambda + \bar{\Lambda})$, and $(\Omega^- + \bar{\Omega}^+)/(\Xi^- + \bar{\Xi}^+)$ as the function of p_T . Experimental data are from [32, 33].

A. p_T spectrum of charm quarks

In Fig. 6(a), we apply the EVC model to fit experimental data for differential cross-section of D^{*+} in pp collisions at $\sqrt{s} = 5.02$ TeV. In the fit, we have used the p_T spectrum of u quarks obtained in previous section and then obtain the p_T distribution of charm quarks at hadronization. In panel (b), we normalize the obtained charm quark distribution and compare it with the perturbative QCD calculation in Fixed-Order Next-to-Leading-Logarithmic (FONLL) scheme [61, 62]. We find a good consistency in the studied p_T range within theoretical uncertainties. By fitting D^{*+} data, we obtain the p_T integrated cross-section of charm quarks $d\sigma_c/dy = 1.0$ mb. This value is higher than the center value of default FONLL calculation $0.461^{+0.58}_{-0.31}$ mb [61, 62] but is still located in its theoretical uncertainties.

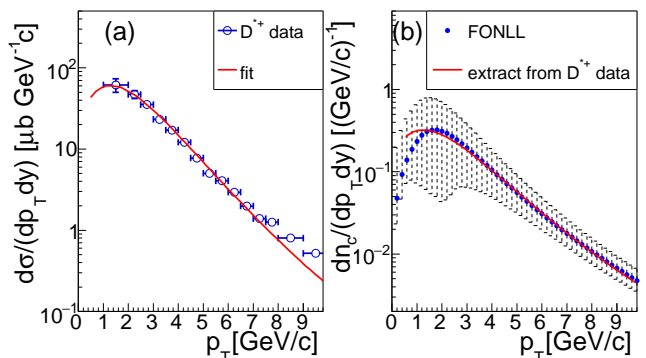


Figure 6. (a) Fit to data of D^{*+} in EVC model. (b) Comparison between the normalized p_T distribution of charm quarks obtained in our model and calculation in FONLL [61, 62].

B. Results of single-charmed hadrons

Using the extracted p_T spectrum of charm quarks in the above subsection and those of light-flavor quarks in Sec. III D, we can calculate p_T spectra of other single-charmed hadrons. In Table I, we firstly present the p_T -integrated cross-section $d\sigma/dy$ of $D^{0,+}$, D_s^+ , Λ_c^+ , $\Xi_c^{0,+}$ and Ω_c^0 in inelastic pp collisions at $\sqrt{s} = 5.02$ TeV. We firstly list analytical expressions and then numerical results as $d\sigma_c/dy = 1.0$ mb and compare with latter with available experimental data [34, 35].

Table I. $d\sigma/dy$ of single-charmed hadrons in EVC model as $d\sigma_c/dy = 1.0$ mb. Strong and electromagnetic decay contributions from other single-charmed hadrons in ground-state have been included. Experimental data are from [34, 35].

$\frac{d\sigma}{dy}$	analytical	numerical (μb)	data (μb)
D^0	$\frac{1+1.677R'_{V/P}}{1+R'_{V/P}} \frac{1}{2+\lambda_s} \frac{1}{1+R_{B/M}^{(c)}} \frac{d\sigma_c}{dy}$	429	447 ± 20
D^+	$\frac{1+0.323R'_{V/P}}{1+R'_{V/P}} \frac{1}{2+\lambda_s} \frac{1}{1+R_{B/M}^{(c)}} \frac{d\sigma_c}{dy}$	181	184 ± 13
D_s^+	$\frac{\lambda_s}{2+\lambda_s} \frac{1}{1+R_{B/M}^{(c)}} \frac{d\sigma_c}{dy}$	91.5	95 ± 9
Λ_c^+	$\frac{4}{(2+\lambda_s)^2} \frac{R_{B/M}^{(c)}}{1+R_{B/M}^{(c)}} \frac{d\sigma_c}{dy}$	225	230 ± 16
Ξ_c^0	$2 \frac{\lambda_s}{(2+\lambda_s)^2} \frac{R_{B/M}^{(c)}}{1+R_{B/M}^{(c)}} \frac{d\sigma_c}{dy}$	33.8	
Ξ_c^+	$2 \frac{\lambda_s}{(2+\lambda_s)^2} \frac{R_{B/M}^{(c)}}{1+R_{B/M}^{(c)}} \frac{d\sigma_c}{dy}$	33.8	
Ω_c^0	$\frac{\lambda_s^2}{(2+\lambda_s)^2} \frac{R_{B/M}^{(c)}}{1+R_{B/M}^{(c)}} \frac{d\sigma_c}{dy}$	5.07	

In Fig. 7, we present results for p_T spectra of $D^{0,+}$, D_s^+ and Λ_c^+ in inelastic pp collisions at $\sqrt{s} = 5.02$ TeV and compare them with experimental data of ALICE collaboration [34, 35]. We find a good agreement for these four hadrons in the low p_T range ($p_T \lesssim 7$ GeV/c). At larger transverse momentum $p_T \gtrsim 8$ GeV/c, results for $D^{0,+}$ in our model are lower than experimental data to a certain extent. This under-estimation maybe indicate the increased importance of fragmentation mechanism for charm quark hadronization at large p_T .

In Fig. 8 (a), we predict p_T spectra of Ξ_c^0 and Ω_c^0 in inelastic pp collisions at $\sqrt{s} = 5.02$ TeV. In comparison with the production of Λ_c^+ , the production of Ξ_c^0 and that of Ω_c^0 are suppressed due to the cascade strangeness. As shown by their p_T -integrated cross-sections in Table I, we have

$$\Lambda_c^+ : \Xi_c^0 : \Omega_c^0 = 1 : \frac{1}{2}\lambda_s : \frac{1}{4}\lambda_s^2, \quad (39)$$

Because $\lambda_s \approx 0.3$ in inelastic pp collisions, we see in Fig. 8 (b) that ratio Ξ_c^0/Λ_c^+ is about 0.1-0.2 and Ω_c^0/Λ_c^+ is about 0.02-0.03 in the low and intermediate p_T range. Ratio

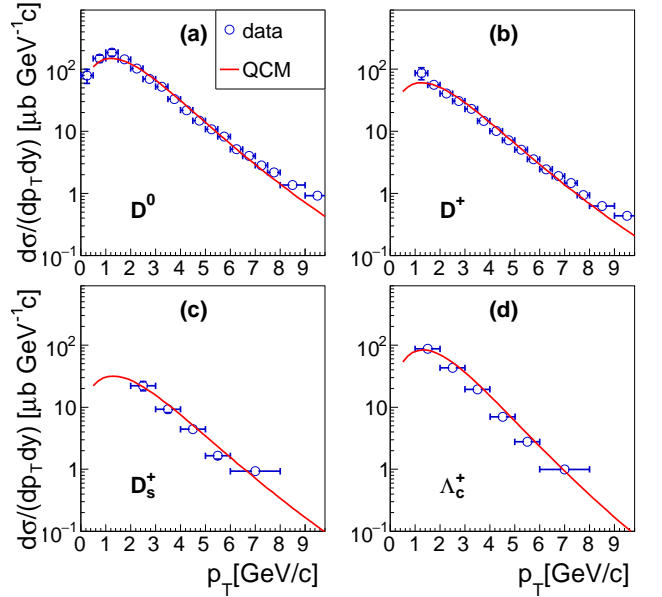


Figure 7. p_T spectra of $D^{0,+}$, D_s^+ and Λ_c^+ at midrapidity in inelastic pp collisions at $\sqrt{s} = 5.02$ TeV. Lines are results of EVC model and symbols are experimental data [34, 35].

Ω_c^0/Ξ_c^0 is also the order of $\lambda_s/2$ and therefore is close to Ξ_c^0/Λ_c^+ . In addition, we see that three ratios all increase with p_T in the low p_T range, which is because the difference between $f_s(p_T)$ and $f_u(p_T)$ as shown in Fig. 4.

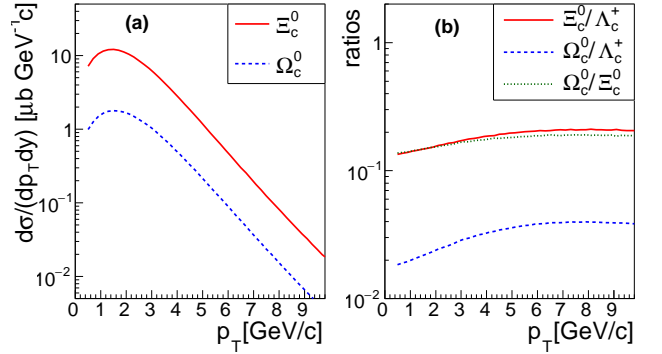


Figure 8. (a) p_T spectra of Ξ_c^0 and Ω_c^0 at midrapidity in inelastic pp collisions at $\sqrt{s} = 5.02$ TeV. (b) Ratios among charmed baryons as the function of p_T .

The ratio of baryon to meson as the function of p_T is sensitive to the production mechanism of hadrons at hadronization. In Fig. 9, we show results for ratios of charmed baryons to charmed mesons as the function of p_T in pp collisions at $\sqrt{s} = 5.02$ TeV. In Fig. 9 (a), we firstly show result of Λ_c^+/D^0 as the solid line. Comparing with experimental data of Λ_c^+/D^0 [34], we see that our model result can well explain the decreasing behavior of experimental data at $p_T \gtrsim 2$ GeV/c. In the low p_T range ($p_T \lesssim 2$ GeV/c), the ratio in our model increases with the increasing p_T . This behavior can be tested in the

future as experimental data in this p_T range are richer and more precise. We note that experimental data of p Pb and Pb-Pb collisions at small p_T have indicated this property [34].

We further present result for $(\Xi_c^0 + \Xi_c^+)/D^0$ in Fig. 9(a) and that for Ω_c^0/D^0 in Fig. 9(b). We see that the magnitude of $(\Xi_c^0 + \Xi_c^+)/D^0$ at $p_T \approx 3$ GeV/c is about 0.16 and that of Ω_c^0/D^0 is only about 0.015. This hierarchy property is due to the cascade strangeness suppression as shown in Eq. (39).

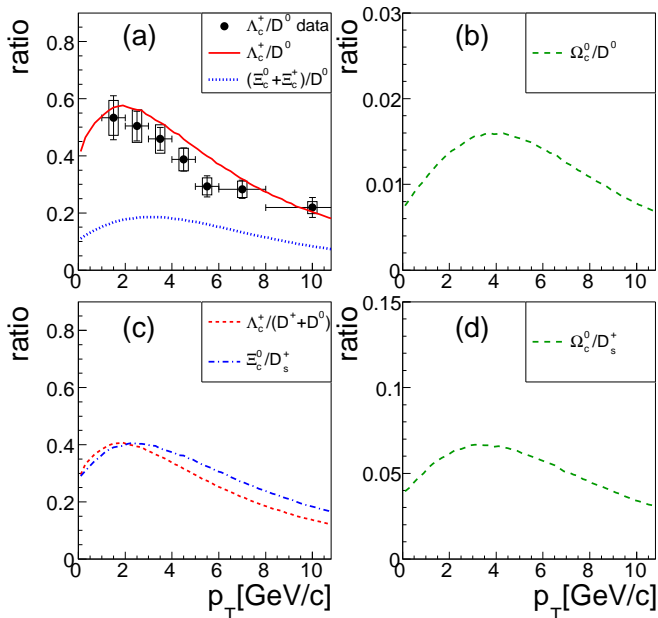


Figure 9. Ratios of charmed baryons to charmed mesons as the function of p_T at midrapidity in inelastic pp collisions at $\sqrt{s} = 5.02$ TeV.

In order to reduce the effect of strangeness suppression and the dependence of model parameters in these baryon to meson ratios, we propose two new ratios $\Lambda_c^+/(D^0 + D^+)$ and Ξ_c^0/D_s^+ . From Table I, two ratios in p_T -integrated cross-sections are of the same magnitude

$$\frac{d\sigma_{\Lambda_c^+}/dy}{d\sigma_{D^0+D^+}/dy} = \frac{d\sigma_{\Xi_c^0}/dy}{d\sigma_{D_s^+}/dy} = \frac{2}{2 + \lambda_s} R_{B/M}^{(c)}. \quad (40)$$

They are independent of model parameter $R'_{V/P}$, which is different from Λ_c^+/D^0 ratio. They are also insensitive to λ_s since the change of λ_s (e.g., 0.3-0.33) only causes little (1%) influence on two ratios. Finally, two ratios directly relate to the production competition of baryon to meson in charm sector which is characterized by the parameter $R_{B/M}^{(c)}$ in our model. Therefore, we propose these two ratios as direct observables of baryon production weight in charm sector. Two ratios as the function of p_T are shown in Fig. 9(c) where we see they are close to each other.

In Fig. 9(d), we show result for Ω_c^0/D_s^+ as the function

of p_T . As indicated by their ratio in p_T -integrated cross-section

$$\frac{d\sigma_{\Omega_c^0}/dy}{d\sigma_{D_s^+}/dy} = \frac{\lambda_s}{2 + \lambda_s} R_{B/M}^{(c)}, \quad (41)$$

this ratio is smaller than Ξ_c^0/D_s^+ by factor $\lambda_s/2$. In addition, we see that the peak position of ratio Ω_c^0/D_s^+ is located at about $p_T \approx 3-4$ GeV/c, which is larger than the peak position of ratios Λ_c^+/D^0 and $\Lambda_c^+/(D^0 + D^+)$ by about 1 GeV/c. This is the kinetic effect caused by the difference between up quark distribution and strange quark distribution shown in Fig. 4.

V. SUMMARY

In this paper, we have applied a quark combination model with equal-velocity combination approximation to study the production of light-flavor hadrons and single-charmed hadrons in pp collisions at $\sqrt{s} = 5.02$ TeV. The systematic comparison with available experimental data indicates the effectiveness of the model, which is consistent with our previous studies in pp collisions at $\sqrt{s} = 7$ and 13 TeV [27–30].

By examining the preliminary data for p_T spectra of Ω and ϕ at midrapidity, we found that two spectra exhibit a quark number scaling property, which gives a first signal for the quark combination mechanism in pp collisions at $\sqrt{s} = 5.02$ TeV. This scaling property further enables us to conveniently extract the p_T spectrum of strange quarks at hadronization. By fitting experimental data of hadrons containing up/down quarks such as proton, we also obtained p_T spectrum of up/down quarks. Using the extracted spectra of up/down and strange quarks, we calculated p_T spectra of K^{*0} , Λ and Ξ which contain both up/down quarks and strange quarks and we found a good agreement with their experimental data. We studied the p_T dependence of the Ω/ϕ ratio and found that the increase/decrease behavior of the ratio with p_T is closely related to the concave/convex shape of the logarithm of strange quark distribution. We also studied the difference between p_T spectrum of up/down quarks and that of strange quarks and used it to explain the difference among p_T spectra of different kinds of baryons.

Using the EVC model, we extracted differential cross-section of charm quarks as the function of p_T by fitting experimental data of D^{*+} . We found it is quite consistent in shape with calculations of perturbative QCD method FONLL. Applying the equal-velocity combination of charm quarks and light-flavor quarks, we successfully explained the experimental data for differential cross-sections of $D^{0,+}$, D_s^+ and Λ_c^+ as the function of p_T . We predicted differential cross-sections of $\Xi_c^{0,+}$ and Ω_c^0 . Compared with Λ_c^+ , production of $\Xi_c^{0,+}$ and Ω_c^0 is suppressed because the abundance of strange quarks at hadronization is suppressed compared with up/down quarks. We predicted ratio $\Xi_c^{0,+}/D^0$ is about 0.16 and Ω_c^0/D^0 is about 0.015 due to the cascade suppress of

strangeness. We also proposed several ratios such as Ξ_c^0/D_s^+ , Ω_c^0/D_s^+ to further show the effect of cascade suppress of strangeness caused by the number of strange quarks involving combination with charm quarks. These predictions can be tested by future experimental data at LHC.

VI. ACKNOWLEDGMENTS

This work is supported in part by Shandong Province Natural Science Foundation under Grants No. ZR2019YQ06 and and No. ZR2019MA053, the National Natural Science Foundation of China under Grant No. 11975011 and No. 11805082, and Higher Educational Youth Innovation Science and Technology Program of Shandong Province (Grants No. 2019KJJ010).

-
- [1] V. Khachatryan *et al.* (CMS), JHEP **09**, 091 (2010), arXiv:1009.4122 [hep-ex].
- [2] S. Chatrchyan *et al.* (CMS), Phys. Lett. **B718**, 795 (2013), arXiv:1210.5482 [nucl-ex].
- [3] V. Khachatryan *et al.* (CMS), Phys. Rev. Lett. **115**, 012301 (2015), arXiv:1502.05382 [nucl-ex].
- [4] V. Khachatryan *et al.* (CMS), Phys. Lett. **B765**, 193 (2017), arXiv:1606.06198 [nucl-ex].
- [5] J. Adam *et al.* (ALICE), Nature Phys. **13**, 535 (2017), arXiv:1606.07424 [nucl-ex].
- [6] J. Adam *et al.* (ALICE), Phys. Lett. **B758**, 389 (2016), arXiv:1512.07227 [nucl-ex].
- [7] J. Adam *et al.* (ALICE), Phys. Lett. **B760**, 720 (2016), arXiv:1601.03658 [nucl-ex].
- [8] B. B. Abelev *et al.* (ALICE), Phys. Lett. **B728**, 25 (2014), arXiv:1307.6796 [nucl-ex].
- [9] M. Luzum and P. Romatschke, Phys. Rev. Lett. **103**, 262302 (2009), arXiv:0901.4588 [nucl-th].
- [10] F.-M. Liu and K. Werner, Phys. Rev. Lett. **106**, 242301 (2011), arXiv:1102.1052 [hep-ph].
- [11] K. Werner, I. Karpenko, and T. Pierog, Phys. Rev. Lett. **106**, 122004 (2011), arXiv:1011.0375 [hep-ph].
- [12] A. Bzdak, B. Schenke, P. Tribedy, and R. Venugopalan, Phys. Rev. **C87**, 064906 (2013), arXiv:1304.3403 [nucl-th].
- [13] P. Bozek and W. Broniowski, Phys. Rev. **C88**, 014903 (2013), arXiv:1304.3044 [nucl-th].
- [14] S. K. Prasad, V. Roy, S. Chattopadhyay, and A. K. Chaudhuri, Phys. Rev. **C82**, 024909 (2010), arXiv:0910.4844 [nucl-th].
- [15] E. Avsar, C. Flensburg, Y. Hatta, J.-Y. Ollitrault, and T. Ueda, Phys. Lett. **B702**, 394 (2011), arXiv:1009.5643 [hep-ph].
- [16] W. Zhao, Y. Zhou, H. Xu, W. Deng, and H. Song, Phys. Lett. B **780**, 495 (2018), arXiv:1801.00271 [nucl-th].
- [17] I. Bautista, A. F. Téllez, and P. Ghosh, Phys. Rev. **D92**, 071504 (2015), arXiv:1509.02278 [nucl-th].
- [18] C. Bierlich, G. Gustafson, L. Lönnblad, and A. Tarasov, JHEP **03**, 148 (2015), arXiv:1412.6259 [hep-ph].
- [19] A. Ortiz Velasquez, P. Christiansen, E. Cuautle Flores, I. Maldonado Cervantes, and G. Paic, Phys. Rev. Lett. **111**, 042001 (2013), arXiv:1303.6326 [hep-ph].
- [20] J. R. Christiansen and P. Z. Skands, JHEP **08**, 003 (2015), arXiv:1505.01681 [hep-ph].
- [21] C. Bierlich and J. R. Christiansen, Phys. Rev. **D92**, 094010 (2015), arXiv:1507.02091 [hep-ph].
- [22] V. Topor Pop, M. Gyulassy, J. Barrette, C. Gale, and A. Warburton, Phys. Rev. C **86**, 044902 (2012), arXiv:1203.6679 [hep-ph].
- [23] V. Minissale, S. Plumari, and V. Greco, (2020), arXiv:2012.12001 [hep-ph].
- [24] S. Gieseke, P. Kirchgaeßer, and S. Plätzer, Eur. Phys. J. C **78**, 99 (2018), arXiv:1710.10906 [hep-ph].
- [25] J. Song, X.-r. Gou, F.-l. Shao, and Z.-T. Liang, Phys. Lett. **B774**, 516 (2017), arXiv:1707.03949 [hep-ph].
- [26] M. He and R. Rapp, Phys. Lett. B **795**, 117 (2019), arXiv:1902.08889 [nucl-th].
- [27] J. Song, H.-h. Li, and F.-l. Shao, Eur. Phys. J. C **78**, 344 (2018), arXiv:1801.09402 [hep-ph].
- [28] X.-r. Gou, F.-l. Shao, R.-q. Wang, H.-h. Li, and J. Song, Phys. Rev. **D96**, 094010 (2017), arXiv:1707.06906 [hep-ph].
- [29] J.-w. Zhang, H.-h. Li, F.-l. Shao, and J. Song, Chin. Phys. **C44**, 014101 (2020), arXiv:1811.00975 [hep-ph].
- [30] H.-H. Li, F.-L. Shao, J. Song, and R.-Q. Wang, Phys. Rev. **C97**, 064915 (2018), arXiv:1712.08921 [hep-ph].
- [31] S. Tripathy (ALICE), Nucl. Phys. A **982**, 180 (2019), arXiv:1807.11186 [hep-ex].
- [32] S. Acharya *et al.* (ALICE), Phys. Rev. C **101**, 044907 (2020), arXiv:1910.07678 [nucl-ex].
- [33] A. M. Sirunyan *et al.* (CMS), Phys. Rev. C **101**, 064906 (2020), arXiv:1910.04812 [hep-ex].
- [34] S. Acharya *et al.* (ALICE), (2020), arXiv:2011.06079 [nucl-ex].
- [35] S. Acharya *et al.* (ALICE), Eur. Phys. J. C **79**, 388 (2019), arXiv:1901.07979 [nucl-ex].
- [36] J. Song, F.-l. Shao, and Z.-t. Liang, Phys. Rev. C **102**, 014911 (2020),

- arXiv:1911.01152 [nucl-th].
- [37] J. Song, H.-h. Li, and F.-l. Shao, Eur. Phys. J. C **81**, 1 (2021), arXiv:2008.03017 [nucl-th].
- [38] J. Song, X.-f. Wang, H.-h. Li, R.-q. Wang, and F.-l. Shao, Phys. Rev. C **103**, 034907 (2021), arXiv:2007.14588 [nucl-th].
- [39] R.-Q. Wang, J. Song, F.-L. Shao, and Z.-T. Liang, Phys. Rev. C **101**, 054903 (2020), arXiv:1911.00823 [hep-ph].
- [40] J. Song and F.-l. Shao, Phys. Rev. C **88**, 027901 (2013), arXiv:1303.1231 [nucl-th].
- [41] F.-l. Shao, G.-j. Wang, R.-q. Wang, H.-h. Li, and J. Song, Phys. Rev. C **95**, 064911 (2017), arXiv:1703.05862 [hep-ph].
- [42] S. Acharya *et al.* (ALICE), JHEP **04**, 108 (2018), arXiv:1712.09581 [nucl-ex].
- [43] K. A. Olive *et al.* (Particle Data Group), Chin. Phys. C **38**, 090001 (2014).
- [44] C. Tsallis, J. Statist. Phys. **52**, 479 (1988).
- [45] K. Garg (ALICE), PoS **LHCP2018**, 054 (2018), arXiv:1811.10916 [hep-ex].
- [46] V. Khachatryan *et al.* (CMS), JHEP **05**, 064 (2011), arXiv:1102.4282 [hep-ex].
- [47] B. B. Abelev *et al.* (ALICE), Eur. Phys. J. C **75**, 1 (2015), arXiv:1406.3206 [nucl-ex].
- [48] B. Abelev *et al.* (ALICE), Phys. Lett. B **712**, 309 (2012), arXiv:1204.0282 [nucl-ex].
- [49] B. I. Abelev *et al.* (STAR), Phys. Rev. **C79**, 064903 (2009), arXiv:0809.4737 [nucl-ex].
- [50] M. M. Aggarwal *et al.* (STAR), Phys. Rev. **C83**, 024901 (2011), arXiv:1010.0142 [nucl-ex].
- [51] B. B. Abelev *et al.* (ALICE), Phys. Rev. Lett. **111**, 222301 (2013), arXiv:1307.5530 [nucl-ex].
- [52] L. Adamczyk *et al.* (STAR), Phys. Rev. C **93**, 021903 (2016), arXiv:1506.07605 [nucl-ex].
- [53] J. Adam *et al.* (STAR), Phys. Rev. C **102**, 034909 (2020), arXiv:1906.03732 [nucl-ex].
- [54] B. Abelev *et al.* (ALICE), Eur. Phys. J. C **72**, 2183 (2012), arXiv:1208.5717 [hep-ex].
- [55] V. Greco, C. M. Ko, and P. Lévai, Phys. Rev. Lett. **90**, 202302 (2003), arXiv:nucl-th/0301093 [nucl-th].
- [56] R. J. Fries, B. Müller, C. Nonaka, and S. A. Bass, Phys. Rev. Lett. **90**, 202303 (2003), arXiv:nucl-th/0301087 [nucl-th].
- [57] R. C. Hwa and C. B. Yang, Phys. Rev. **C67**, 034902 (2003), arXiv:nucl-th/0211010 [nucl-th].
- [58] L.-W. Chen and C. M. Ko, Phys. Rev. **C73**, 044903 (2006), arXiv:nucl-th/0602025 [nucl-th].
- [59] C.-e. Shao, J. Song, F.-l. Shao, and Q.-b. Xie, Phys. Rev. **C80**, 014909 (2009), arXiv:0902.2435 [hep-ph].
- [60] R.-q. Wang, F.-l. Shao, J. Song, Q.-b. Xie, and Z.-t. Liang, Phys. Rev. C **86**, 054906 (2012), arXiv:1206.4373 [hep-ph].
- [61] M. Cacciari, M. Greco, and P. Nason, JHEP **05**, 007 (1998), arXiv:hep-ph/9803400.
- [62] M. Cacciari, S. Frixione, and P. Nason, JHEP **03**, 006 (2001), arXiv:hep-ph/0102134.